Optics Letters

Miniaturized spectroscopy with tunable and sensitive plasmonic structures

Li Liang,[1,2,3,†] Qilin Zheng,[2,†] Long Wen,[2] David R. S. Cumming,[4] and Qin Chen[2,*]

[1]School of Nano-Tech and Nano-Bionics, University of Science and Technology of China, Hefei 230026, China
[2]Institute of Nanophotonics, Jinan University, Guangzhou 511443, China
[3]Suzhou Institute of Nano-Tech and Nano-Bionics, Chinese Academy of Sciences, Suzhou 215123, China
[4]James Watt School of Engineering, University of Glasgow, Glasgow G12 8QQ, UK
*Corresponding author: chenqin2018@jnu.edu.cn

Received 2 April 2021; revised 8 June 2021; accepted 2 July 2021; posted 2 July 2021 (Doc. ID 426624); published 25 August 2021

A broad linewidth and a lack of spectral analysis limit the applications of plasmonic sensors. In this Letter, a plasmonic sensor with a large sensitivity in the terahertz (THz) range is proposed based on high-quality factor (>1000) surface lattice resonance in subwavelength near-flat metallic gratings. Moreover, such a highly selective spectral manipulating scheme, plus the greatly localized plasmonic resonance, enables miniaturized spectroscopy based on a single detector by integrating an electro-optical material with the gratings. A spectral resolution of 0.1 GHz at a center frequency of 1.1 THz is predicted showing a four times improvement of measuring efficiency. This technique shows promising potential in on-site matter inspection and point-of-care testing.

https://doi.org/10.1364/OL.426624

Plasmonic sensors rely on the detection of the surface plasmon resonance shift as an indication of a change of the surrounding dielectric refractive index induced by the biochemical reactions or the target species [1,2]. The larger the spatial overlap between the electromagnetic fields and the analytes, the larger the sensitivity (S), defined as the resonant wavelength or frequency shift ($\Delta\lambda$ or Δf) divided by the index variation (Δn). Although the sensitivity is an important performance parameter to evaluate optical sensors, the actual detection limit is strongly associated with the spectral linewidth of the resonance. Therefore, a figure of merit (FoM) defined as sensitivity divided by the resonance linewidth (FWHM) is proposed as an overall performance index [3]. Plasmonic sensors usually show larger sensitivities than other optical sensors such as waveguide sensors [4], photonic crystal sensors [5] and microcavity sensors [6], but they suffer from high absorption loss, i.e., a large resonance linewidth. The quality (Q) factors defined as the resonance wavelength (λ) or frequency (f) divided by the resonance linewidth of plasmonic sensors are always several tens [7]. As a result, the FoMs of plasmonic sensors are usually very limited, for example, Akowuah *et al.* proposed a plasmonic waveguide sensor with a sensitivity of 4300 nm/refractive index unit (RIU), but the FoM is limited to 20 RIU^{-1} by the high loss of the propagating surface plasmon resonance [8]. Hu *et al.* proposed a plasmonic sensor working in a flowing-through model with an ultrahigh sensitivity of 3.5 terahertz (THz)/RIU in a THz range, but its FoM is less than 10 RIU^{-1} due to its low Q-factor resonance [9]. A dielectric resonator usually has much larger Q-factors, for example, photonic crystal sensor [5] has an extremely high Q-factor over 10000, but its FoM is only 19 RIU^{-1} due to an extremely low sensitivity limited by the interaction between the weak evanescent optical field and the analyte. Furthermore, a sensor based on an ultrahigh Q-resonator usually needs an extra temperature control module and high-resolution spectrometer, which limits its actual applications for point-of-care (POC) diagnosis and on-site inspection. It is also noted that conventional plasmonic sensors can only detect the variation of a refractive index and therefore lack the ability for matter inspection, in particular isomers. In contrast, spectroscopy is an effective method to recognize the spectral fingerprints of target molecules [10,11]. With the development of nanophotonics and nanofabrication techniques, microspectrometers have been demonstrated in the visible and infrared band [12,13]. Although the THz range has plenty of spectral fingerprint information, current commercial THz spectroscopy systems are usually bulky, complex, and expensive. Little work has been reported on THz microspectrometers [14]. It is important to develop a high-efficiency and miniaturized platform for THz sensing and spectroscopy. Considering the complexity and cost of a THz detector array, microspectrometers based on a single detector or a small number of detectors are more attractive.

In this Letter, a plasmonic sensor with an ultrahigh FoM over 900 RIU^{-1} in the THz range is proposed based on subwavelength near-flat metallic gratings. A strong interaction between the surface resonances and the THz beam results in a remarkable normalized sensitivity ($S' = S/f$) of 0.9 RIU^{-1}, and the suppressed radiative and absorption loss with the near-flat grating structure allows an ultrahigh Q-factor above 1000. The plasmonic resonance can be readily tuned across the whole THz band keeping its narrowband feature. By integrating such subwavelength metallic gratings with electro-optical materials,

miniaturized spectroscopy is demonstrated by reconstructing the original spectrum based on compressive sensing (CS) algorithm, where the spectral resolution reaches 0.1 GHz at a center frequency of 1.1 THz. Multi-resonance structures and resonator multiplexing are investigated and discussed to extend the spectral operating range.

To increase the FoM of plasmonic sensors, the key issue is to reduce the loss in plasmonic structures. In an optical resonant system, there are basically two main loss factors, including the absorption loss and the radiative loss. Dielectric microcavities, for example, a toroid microcavity, have extremely high Q-factors up to 10^8, because there are negligible absorption loss (lossless material) and ultralow radiative loss (smooth whispering gallery profile) [15]. In contrast, most plasmonic resonant structures suffer from the serious ohmic loss (lossy metals) and radiative loss (leaky modes) [8,9]. As the Q-factor is determined by the sum of both losses, it is important to simultaneously suppress the two lossy channels for improving the Q-factor.

A simple plasmonic resonant structure consisting of optically thick Au film covered subwavelength one-dimensional (1D) silicon gratings is proposed, as shown in Fig. 1(a). When transverse-magnetic polarized light normally illuminates on such a mirror-like structure, a plasmonic resonance is excited, resulting in a reflection minimum, as shown in Fig. 1(b). By adjusting the grating period, the resonance frequency can be tuned, which keeps its narrowband feature. The electric and magnetic field distributions are shown in Figs. 1(d) and 1(e), indicating a surface resonance with strong field components at the surface. Both strong dependency of the resonance wavelength on the grating period and the diffractive mode-like field distributions agree well with the mode properties of surface lattice resonance (SLR, Supplement 1) [16,17], which is also referred to as Rayleigh anomaly. The distribution of energy flow density and the Poynting vectors (white arrows) are shown in Fig. 1(f). The energy flow density concentrates on the surface of gratings, and the Poynting vectors form two vortices, which traps the incident beam close to the grating surface and reduces the reflection. To evaluate the influence of the absorption loss and radiative loss on the resonance linewidth, the structure can be qualitatively represented by a one-port resonator within the framework of the temporal coupled mode theory (CMT, Supplement 1). Figure 1(c) shows the calculated $1/\tau_a$ and $1/\tau_r$ for structures with different grating widths w_g and depth h,

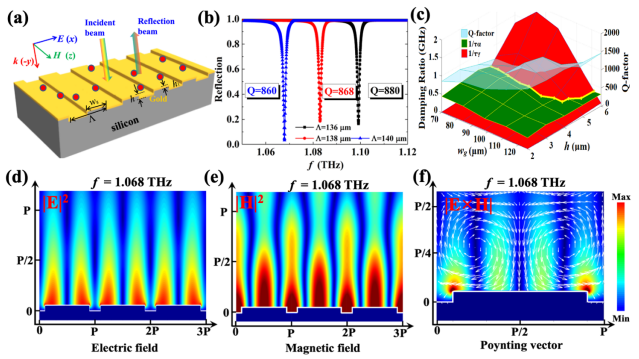

Fig. 1. Grating height $h = 5.5$ μm, Au thickness $h_1 = 200$ nm, grating width $w_g = 116$ μm, and environmental refractive index $n = 2.0$. (c) Calculated Q-factors and damping ratios $1/\tau_a$ and $1/\tau_r$ for different w_g, and h. $\Lambda = 140$ μm; the other parameters are the same as (b). (d) Electric field, (e) magnetic field, and (f) energy flow density and Poynting vectors at resonance ($f = 1.068$ THz).

where $1/\tau_a$ and $1/\tau_r$ are the damping ratios related to absorption loss and radiative loss. As seen, the absorption loss remains basically unchanged, because it is mainly determined by the metal material properties, but the radiative loss decreases rapidly with the decreasing h, because the leaky mode becomes cutoff. In the case of critical coupling indicated by the dotted line, i.e., $1/\tau_a = 1/\tau_r$, zero-reflection is achieved at the resonance resulting in a strong interaction between the incident light and the structure. In the whole structure parameter space, the Q-factor is mainly determined by the larger one between $1/\tau_a$ and $1/\tau_r$. For shallow gratings with $h < 4$ μm ($<1/60\lambda$), the absorption loss dominates the total loss, and the Q-factor saturates. As shown in Fig. 1(b), high Q-factors above 860 are easily obtained for such plasmonic THz sensors. By carefully optimizing the structural parameters ($h = 2$ μm, $w_g = 126$ μm), an ultrahigh Q-factor of 1650 can be obtained as shown in Fig. 1(c), which is finally limited by the material absorption.

It is shown in Fig. 1 that plasmonic resonances with ultrahigh Q-factors and strongly localized surface electromagnetic fields can be achieved in a simple subwavelength metal grating structure. It is expected that such a structure enables excellent sensing performance. As shown in Fig. 2(a), increasing the refractive index of the analyte above the gratings causes obvious red shift of the resonance. A sensitivity as high as 1.8 THz/RIU is achieved around 2 THz. At the same frequency, the Q-factor exceeds 1000, which is one or two orders of magnitude larger than conventional plasmonic [7] or metamaterial sensors [9]. The remarkable sensitivity is associated with the large spatial overlap between the surface resonant fields and the analyte, which is difficult to be realized in microcavity and photonic crystal sensors. Due to the high Q-factor and the large sensitivity, the metallic shallow grating sensor demonstrates an ultrahigh FoM over 900 RIU^{-1}. In Fig. 2(b), the Q-factor and the normalized sensitivity S' of various THz sensors are plotted for comparison. S' is used to exclude the influence of the working frequency of different sensors. Each FoM is the

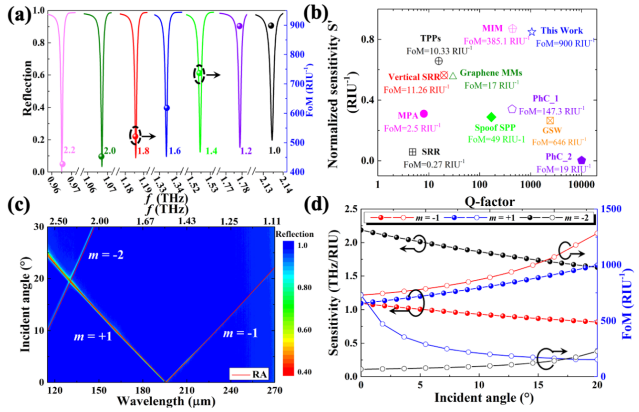

Fig. 2. (a) Simulated reflection spectra and FoM versus n. $\Lambda = 140$ μm, $h = 5.5$ μm, $h_1 = 200$ nm, and $w_g = 116$ μm. (b) Comparison of various THz sensors, including spoof surface plasmon–polaritons (SPPs) [24], photonics crystal (PhC) [5,25], metamaterial perfect absorbers (MPAs) [9], graphene metamaterial (MM) [26], split ring resonators (SRRs) [27], vertical SRRs [28], Tamm plasmon–polaritons (TPPs) [18], metal-insulator-metal (MIM) [20], grating slot waveguides (GSWs) [19]. (c) Simulated reflection spectra versus incident angle θ, where the red lines represent the dispersion relation of RA. $n = 1.4$, and the other parameters are the same as (a). (d) Predicted sensitivity and FoM at oblique incidence.

product of the horizontal coordinate and the longitudinal coordinate. The metallic shallow grating sensor in this Letter demonstrates a high FoM because of both its high Q-factor of 1050 and high S' of 0.9 RIU^{-1}. In contrast, although other sensors may have either a high Q-factor or high S', they do not possess a high Q-factor and high S' simultaneously. For example, both the metamaterial absorber based flowing-through sensor [9] and the Tamm plasmon sensor [18] have small FoMs around 10 RIU^{-1} due to their large radiative loss, although they have decent sensitivities. A photonic crystal sensor [5] has an extremely high Q-factor over 10000, but its FoM is only 19 RIU^{-1} due to an ultralow S' of 0.0019 RIU^{-1} limited by the interaction between the weak evanescent optical field and the analyte. A grating slot waveguide sensor shows a high FoM above 600 RIU^{-1}, but the device fabrication relies on complex wafer bonding [19]. A metal-insulator-metal (MIM) sensor needs accurate control of the dielectric layer thickness [9,20]. In contrast, the metallic shallow grating sensor is very simple and easy for fabrication and integration with microfluidics. This result shows great potential of such a sensing platform in matter inspection and biomedical diagnosis. The above analysis focuses on the first-order diffraction induced plasmonic resonance at normal incidence. As shown in Fig. 2(c), the resonance splits into two absorption bands and the frequency difference between the two bands increases rapidly with the increasing incident angle (Supplement 1). With the increasing incident angle, the sensitivity of the negative order reduces while the positive one grows. Although the sensitivity of the -2 order coupled mode is higher than that of the first-order one, its linewidth is much larger, resulting in a smaller FoM.

All the optical sensors in Fig. 2(b) are refractive index sensors, i.e., they work by detecting the index variation, but cannot differentiate the analytes in a complex analyte. Alternatively, spectroscopy is a widely used technique for matter inspection, in particular in the infrared or THz range full of spectral fingerprint. Usually, a spectrum is obtained by collecting light intensity at a series of frequencies, which can be realized by rotating diffractive gratings in front of a pin hole covered photodetector. Recently, microspectrometers have attracted broad interests due to the advantages in weight, size, and cost [10,11]. It is usually realized by integrating a series of filters such as quantum dots [21], metasurfaces [12], and photonic crystals [11] with an array of detectors (e.g., CMOS image sensors), where each pair of filters and detectors collects the signal of a target spectrum in a certain frequency range. By combining all these signals, the whole spectral information is obtained by using the CS technique with a high resolution and efficiency. However, the multi-pixel THz detector array is expensive and complex, which may impede the practical application of this technique.

The high sensitivity of the plasmonic sensors discussed above predicts efficient spectral tuning by adjusting the environmental refractive index on the sensor surface, as shown in Fig. 2(a). By incorporating light modulation with an active material (e.g., liquid crystal [22]) in such a plasmonic sensing structure, a miniaturized THz spectrometer is expected with a single THz detector at a low cost by successively sampling the target spectrum via electrically tuning the spectral response of the plasmonic structure. High spectral reconstruction accuracy and efficiency can be expected due to the high FoM of the proposed plasmonic structure. In this case, at each step, the spectral information is sampled at a certain frequency, which is similar to a scanning grating spectrometer. If multiple resonances can be formed in such a structure, spectral information at multiple frequencies can be collected at each step, which may speed up the measurement process. As seen from Fig. S1 in Supplement 1, multiple resonances at customized frequencies can be easily constructed by either asymmetric 2D gratings or oblique incidence, which can be easily tuned by electrically gating the active material on the surface of the metal gratings (see supporting information in Supplement 1). To demonstrate the benefits of multiple resonances, two types of SLR structures with single resonance and three resonances are designed as shown in Fig. S2 in Supplement 1. A series of filtering responses of these plasmonic structures are shown in Fig. S2(a)–(b) in Supplement 1 by electrically tuning the refractive index of liquid crystal [22,23], where these figures actually compose the response matrixes for spectrum reconstruction via the CS algorithm (Supplement 1). It is obvious that increasing the data points in the figures, i.e., more spectral information sampling, requires more reflection intensity measurements. Three-resonance structures certainly have advantages over the single-resonance one, because the spectral information is sampled at several regions simultaneously each time. Fig. S2(c)–(d) in Supplement 1 show the reconstructed spectra with these two plasmonic structures, where a target spectrum (black line) is reconstructed at different sampling (voltage tuning) times. It is found that a data set of 50 times sampling, i.e., reflected intensity measurement with the tunable plasmonic structure at 50 different voltages, almost fully reconstructs the target spectrum when the single-resonance structure is used, as shown in Fig. S2(c) (Supplement 1). Obvious deviations are observed when the sampling times reduce to 25. In contrast, the spectrum reconstruction with three-resonance structures is realized with fewer sampling times. For example, 25 times sampling is enough to fully recover the target spectrum as shown in Fig. S2(d) (Supplement 1). Moreover, the multi-resonance structure can not only improve the measuring efficiency, as shown in Fig. S2 in Supplement 1, but also it can extend the working spectral range. Generally, the spectral operating range of such an approach is determined by the frequency shift of tunable resonators, which is finally limited by the refractive index tuning range, for example, 0.2 for common liquid crystals [23]. Alternatively, the operating range can be extended by introducing multi-resonance in a single grating structure to cover a broader spectral range. As shown in Fig. S3(a)–(c) in Supplement 1, the four-resonance structure covers a larger spectral range than that of the single-resonance and dual-resonance ones. As a result, it can fully reconstruct the target spectrum as shown in Fig. S3(d) in Supplement 1, but the other two show significant deviations due to the lack of complete spectral information in the sampled data.

To evaluate the performance of the proposed miniaturized THz spectrometer, the operating bandwidth and the spectral resolution are two important parameters. By multiplexing several such multi-resonance structures working in different spectral ranges, the spectral operating range is expected to be extended. As shown in Fig. 3(a), three four-resonance plasmonic structures are matched to cover a spectral operating range of 1 THz around a central frequency of 1.5 THz. Nearly perfect spectral reconstruction is obtained with only 20 times sampling, as shown in Fig. 3(b). To demonstrate the spectral resolution of this technique, reconstruction of a spectrum with two close narrowband peaks ($\Delta f = 0.1$ GHz) is conducted

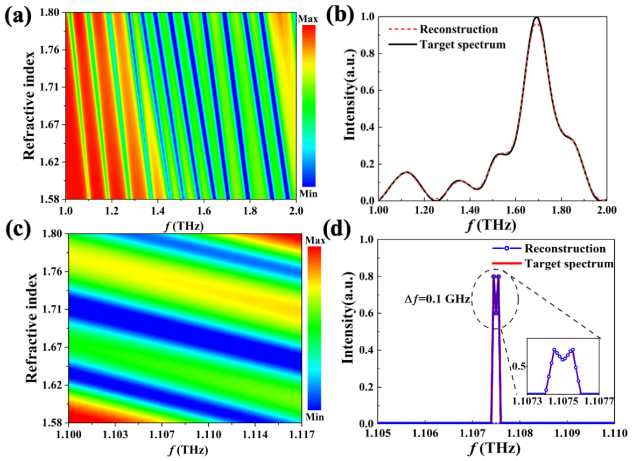

Fig. 3. (a) Spliced simulated reflection spectra of three four-resonance plasmonic structures versus the refractive index of liquid crystal by tuning the driving voltage. $\Lambda_{x1} = 120\ \mu\text{m}$, $\Lambda_{y1} = 138\ \mu\text{m}$, $w_{gx1} = 0.8\ \Lambda_{x1}$, $w_{gy1} = 0.8\ \Lambda_{y1}$; $\Lambda_{x2} = 194\ \mu\text{m}$, $\Lambda_{y2} = 210\ \mu\text{m}$, $w_{gx2} = 0.8\ \Lambda_{x2}$, $w_{gy1} = 0.8\ \Lambda_{y2}$; $\Lambda_{x3} = 226\ \mu\text{m}$, $\Lambda_{y3} = 240\ \mu\text{m}$, $w_{gx3} = 0.8\ \Lambda_{x1}$, $w_{gy3} = 0.8\ \Lambda_{y1}$; $h = 6.0\ \mu\text{m}$ and incident angle $\theta = 14°$. (b) Reconstructed spectrum of a target spectrum with the spectral responses in (a). (c) Simulated reflection spectra of a three-resonance plasmonic structure versus the refractive index of liquid crystal at different driving voltages. $\Lambda_x = 220\ \mu\text{m}$, $w_{gx} = 176\ \mu\text{m}$, $\Lambda_y = 218\ \mu\text{m}$, $w_{gy} = 174\ \mu\text{m}$, $h = 6.0\ \mu\text{m}$, and incident angle $\theta = 3.0°$. (d) Reconstructed spectrum of a narrowband target spectrum with the spectral responses in (c).

with a three-resonance structure, as shown in Fig. 3(c). The predicted spectral resolution is compatible to the commercial spectrometers. Moreover, it is seen that the distinct dual-peak spectral profile is fully resolved by only 25 times sampling. In contrast, at least 100 data points in the same frequency range are required to differentiate these two peaks in a conventional working model with uniform point-by-point sampling scheme-like grating spectrometers. It means roughly four times improvement of the measuring efficiency. All these results confirm the decent performance of such a novel miniaturized spectroscopy technique based on a tunable and sensitive plasmonic structure, and show promising potential for applications in on-site matter inspection and POC diagnosis.

To summarize, we have proposed an ultrahigh FoM plasmonic sensor in the THz range and further demonstrated a novel miniaturized spectroscopy technique based on such a highly selective spectral manipulating scheme. Both a large spectral sensitivity and high Q-factor are important for improving the FoM, which are achieved in a simple near-flat metallic grating structure with significantly localized electromagnetic fields and low loss. Benefiting from the large refractive index sensitivity, this structure can be turned into an effective tunable filter by integrating it with electro-optical materials. As a result, a reconstructed spectrum with high resolution can be obtained by successively sampling the target spectrum with the tunable plasmonic structure and processing with a CS technique. It is expected that these advantages will enable it to be a potential tool in on-site matter inspection and POC testing.

Funding. National Key Research and Development Program of China (2019YFB2203402); National Natural Science Foundation of China (11774383, 11774099, 11874029, 92050108); Guangdong Science and Technology Program International Cooperation Program (2018A050506039, 2021A0505030038); Guangdong Basic and Applied Basic Research Foundation (2020B1515020037); Pearl River Talent Plan Program of Guangdong (2019QN01X120); Royal Society Newton Advanced Fellowship at University of Glasgow (NA140301); Engineering and Physical Sciences Research Council (EP/T00097X/1).

Disclosures. The authors declare no conflicts of interest.

Data Availability. Data are available on request from the authors.

Supplemental document. See Supplement 1 for supporting content.

[†]These authors contributed equally to this Letter.

REFERENCES

1. R. Jha and A. K. Sharma, Opt. Lett. **34**, 749 (2009).
2. H. Im, H. Shao, Y. I. Park, V. M. Peterson, C. M. Castro, R. Weissleder, and H. Lee, Nat. Biotechnol. **32**, 490 (2014).
3. P. Offermans, M. C. Schaafsma, S. R. K. Rodriguez, Y. Zhang, M. Crego-Calama, S. H. Brongersma, and J. G. Rivas, ACS Nano **5**, 5151 (2011).
4. V. Astley, K. S. Reichel, J. Jones, R. Mendis, and D. M. Mittleman, Appl. Phys. Lett. **100**, 231108 (2012).
5. C. Zhang, S. Shen, Q. Wang, M. Lin, Z. Ouyang, and Q. Liu, Materials **13**, 1217 (2020).
6. S. Krämmer, S. Rastjoo, T. Siegle, S. F. Wondimu, C. Klusmann, C. Koos, and H. Kalt, Opt. Express **25**, 7884 (2017).
7. Y. Chen and H. Ming, Photonics Sens. **2**, 37 (2012).
8. E. K. Akowuah, T. Gorman, and S. Haxha, Opt. Express **17**, 23511 (2009).
9. X. Hu, G. Xu, L. Wen, H. Wang, Y. Zhao, Y. Zhang, D. R. S. Cumming, and Q. Chen, Laser Photonics Rev. **10**, 962 (2016).
10. F. Yesilkoy, E. R. Arvelo, Y. Jahani, M. Liu, A. Tittl, V. Cevher, Y. Kivshar, and H. Altug, Nat. Photonics **13**, 390 (2019).
11. Z. Wang, S. Yi, A. Chen, M. Zhou, T. S. Luk, A. James, J. Nogan, W. Ross, G. Joe, A. Shahsafi, K. X. Wang, M. A. Kates, and Z. Yu, Nat. Commun. **10**, 1020 (2019).
12. A. Tittl, A. Leitis, M. Liu, F. Yesilkoy, D. Choi, D. N. Neshev, Y. S. Kivshar, and H. Altug, Science **360**, 1105 (2018).
13. Q. Chen, L. Liang, Q. Zheng, Y. Zhang, and L. Wen, Opto-Electron. Adv. **3**, 190040 (2020).
14. T. Yang, Y. Zhang, J. Ge, L. Wang, Y. Qin, Y. Zhu, W. Huang, and H. Ho, Opt. Lett. **44**, 6061 (2019).
15. D. K. Armani, T. J. Kippenberg, S. M. Spillane, and K. J. Vahala, Nature **421**, 925 (2003).
16. M. Manjappa, Y. K. Srivastava, and R. Singh, Phys. Rev. B **94**, 161103 (2016).
17. L. Wen, L. Liang, X. Yang, Z. Liu, B. Li, and Q. Chen, ACS Nano **13**, 6963 (2019).
18. M. M. Keshavarz and A. Alighanbari, Photonics Res. **58**, 3604 (2019).
19. L. Liang, X. Hu, L. Wen, Y. Zhu, X. Yang, J. Zhou, Y. Zhang, I. E. Carraza, J. Grant, C. Jiang, D. R. S. Cumming, B. Li, and Q. Chen, Laser Photonics Rev. **12**, 1800078 (2018).
20. B. X. Wang, W. Q. Huang, and L. L. Wang, RSC Adv. **7**, 42956 (2017).
21. J. Bao and M. G. Bawendi, Nature **523**, 67 (2015).
22. C. Chen, C. Hsieh, Y. Lin, R. Pan, and C. Pan, Opt. Express **12**, 2625 (2004).
23. L. Wang, X. Lin, X. Liang, J. Wu, W. Hu, Z. Zheng, B. Jin, Y. Qin, and Y. Lu, Opt. Mater. Express **2**, 1314 (2012).
24. H. Yao and S. Zhong, Opt. Express **22**, 25149 (2014).
25. K. Okamoto, K. Tsuruda, S. Diebold, S. Hisatake, M. Fujita, and T. Nagatsuma, J. Infrared, Millimeter, Terahertz Waves **38**, 1085 (2017).
26. C. Liu, P. Liu, C. Yang, and L. Bian, J. Opt. **19**, 115102 (2017).
27. Y. K. Srivastava, L. Cong, and R. Singh, Appl. Phys. Lett. **111**, 201101 (2017).
28. W. Wang, F. Yan, S. Tan, H. Zhou, and Y. Hou, Photonics Res. **5**, 571 (2017).